J. Fluid Mech. (1995), *vol.* 299, *pp.* 389–405

Non-equilibrium dissociating flow over spheres

By C.-Y. WEN[1] AND H. G. HORNUNG[2]

[1] Department of Mechanical Engineering, Da-Yeh Institute of Technology, Taiwan.

[2] Graduate Aeronautical Laboratories, California Institute of Technology, Pasadena, CA 91125, USA

(Received 27 May 1994 and in revised form 10 May 1995)

Previous work on the correlation of dissociative non-equilibrium effects on the flow field in front of blunt bodies considered the dependence of the dimensionless shock stand-off distance on the dimensionless dissociation rate immediately after the normal shock in the simple case of a diatomic gas with only one reaction. In this paper, the correlation is corrected to take into account the additional parameter of the dimensionless free-stream kinetic energy, and extended to the case of complex gas mixtures with many species and many reactions, by introducing a new reaction rate parameter that has a clear physical meaning, and leads to an approximate theory for the stand-off distance. Extensive new experimental results and numerical computations of air, nitrogen and carbon dioxide flow over spheres were obtained over a large range of total enthalpy. The results comprise surface heat flux measurements and differential interferograms. Both experimental results and numerical computations substantiate the approximate theory.

1. Introduction

When a sphere is placed in a flow at high Mach number and at such high velocity that the ordered kinetic energy of the uniform free stream is comparable with the dissociation energy of the gas, two new parameters (in addition to those of perfect-gas flows) enter the problem. In the simplest case of dissociation of a single diatomic gas, a dimensionless number of the form $K \equiv u_\infty^2/(2D)$ measures the free-stream kinetic energy in terms of the dissociation energy of the gas. Here, u_∞ is the free-stream speed and D is the specific dissociation energy of the gas.

If the gas density is sufficiently large, the collision frequency between the molecules is high and produces a dissociation rate that is fast enough to cause significant dissociation over distances that are comparable with the diameter of the sphere. In the simplest case of dissociation of a single diatomic gas, where the composition may be characterized by a single variable, e.g. the dissociation fraction α, this means that a dimensionless number of the form

$$\Omega \equiv \left(\frac{\mathrm{d}\alpha}{\mathrm{d}t}\right)_s \frac{d}{2u_\infty}$$

is $O(1)$. Here, the time derivative is the dissociation rate at a representative point, e.g. just after the normal shock wave, and d is the diameter of the sphere. High density is required to satisfy this condition because the dissociation rate is directly proportional to the density. Clearly, this means that the product of density and body size has to be sufficiently large. Hence, the Reynolds number of the flow is also large, and for

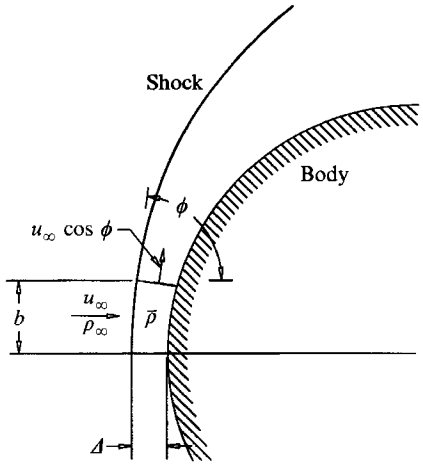

FIGURE 1. Schematic of control volume, and notation.

many purposes the flow may be considered to be inviscid to very good approximation. Infinite Ω corresponds to such a fast reaction that the flow may be considered to be in equilibrium, while zero Ω corresponds to no dissociation, or the frozen limit. For given free-stream conditions, Ω can be varied by changing the size of the body.

A well-known feature of hypervelocity blunt-body flows is that the shock wave stand-off distance Δ is inversely proportional to the average density on the stagnation streamline. This follows from a very simple argument which is presented here because it determines the right dimensionless numbers to choose for the problem. Consider the control volume shown in figure. 1. Apply continuity to this control volume. At the left, the rate at which mass enters the control volume is $u_\infty \rho_\infty b$, or $\pi u_\infty \rho_\infty b^2$, depending on whether the flow is plane or axisymmetric. For small b, the rate at which mass leaves the control volume is $u_b \bar{\rho} \Delta$ or $2\pi u_b b \bar{\rho} \Delta$, respectively, where $\bar{\rho}$ is the average density in the shock layer. With $u_b \approx u_\infty \cos\phi$ and $b = r_s \cos\phi$, mass balance gives

$$\frac{1}{2}\frac{\Delta}{r_s}\frac{\bar{\rho}}{\rho_\infty} = \frac{1}{4} \quad \text{and} = \frac{1}{2}$$

respectively, for axisymmetric and plane flow. Here, r_s is the radius of curvature of the shock. Since the stand-off distance is small compared to the body radius, $d/2 \approx r_s$ and the dimensionless parameter on the left may be formed with the body radius instead of the shock radius. The importance of this simple argument is not in the numbers on the right, but in the fact that it brings out the importance of the average density in the shock layer.

This topic was studied theoretically and experimentally in some detail by Hornung (1972). By examining a large number of numerical computations of dissociating flow over cylinders, it was found that the dimensionless stand-off distance, in the form

$$\tilde{\Delta} \equiv \frac{\Delta}{d}\frac{\rho_s}{\rho_\infty},$$

could be correlated by plotting it against the parameter Ω. Here, ρ_s is the density immediately after the normal shock. The computed density fields in the shock layer were also shown to be correlated approximately by Ω. However, the experimental

results of that study, obtained in the free-piston shock tunnel, T3, at the Australian National University, did not corroborate the numerical correlation very well.

This earlier study suffered from two main problems. First, the theory was limited to a single diatomic gas, and did not account for the effect of K on $\widetilde{\Delta}$. No derivation of the correlation of $\widetilde{\Delta}$ with Ω was given. Second, the unavoidable end-effects in experimental studies of flow over cylinders manifest themselves in just the same manner as non-equilibrium dissociation effects, so that the latter were obscured by them. Also, the facility employed probably suffered from driver-gas contamination at the highest specific enthalpies tested.

Therefore, in the present study, we have the following three aims: to perform a theoretical study to relate the stand-off distance to both Ω and K; to seek a more general reaction rate parameter, that allows the gas to consist of many species with many reactions; and to test the results experimentally and numerically. In the experiments, the new facility T5, at GALCIT, in which the density is significantly larger than was possible in T3 so that interferograms of flow over spheres give sufficient resolution, permitted the bothersome problems associated with flow over cylinders to be avoided. In the numerical investigation, the code developed by Candler (1988) was employed.

2. Conditions along the stagnation streamline

2.1. *Effect of chemical reactions*

Consider the stagnation streamline along the symmetry axis between the shock and the stagnation point. The momentum and energy equations for inviscid adiabatic flow take the simple forms

$$\mathrm{d}p + \rho u \mathrm{d}u = 0 = \mathrm{d}h + u\mathrm{d}u,$$

where p, ρ, u, and h are pressure, density, velocity and specific enthalpy respectively. Thus,

$$\mathrm{d}p = \rho \mathrm{d}h \ .$$

This equation does not mean that the entropy is constant along the stagnation streamline, but rather that the only entropy change that occurs is that associated with the chemical reaction:

$$T\mathrm{d}s = \sum \hat{\mu}_i \mathrm{d}c_i \ ,$$

where T, s are temperature and specific entropy, and the $\hat{\mu}_i$ and c_i are the chemical potentials and mass fractions of the constituents. Let the caloric equation of state be given in the form

$$h = h(p, \rho, c_i) \ .$$

Since the mass fractions must satisfy the identity

$$\sum_{i=1}^{n} c_i = 1 \ ,$$

the number of mass fractions that are independent is one less than the total number n of components present. It is usually convenient to choose c_1 as a dependent variable

and the other c_i as independent variables. Thus,

$$\mathrm{d}h = h_\rho \mathrm{d}\rho + h_p \mathrm{d}p + \sum_{i=2}^{n} h_{c_i} \mathrm{d}c_i = h_\rho \mathrm{d}\rho + \rho h_p \mathrm{d}h + \sum_{i=2}^{n} h_{c_i} \mathrm{d}c_i ,$$

where the subscripts denote partial differentiation. Solving for $\mathrm{d}\rho$,

$$\mathrm{d}\rho = \frac{1-\rho h_p}{h_\rho} \mathrm{d}h - \frac{1}{h_\rho} \sum_{i=2}^{n} h_{c_i} \mathrm{d}c_i \ .$$

Note that the coefficient of $\mathrm{d}h$ is related to the frozen speed of sound a_f, and that $\mathrm{d}h$ may be replaced by $-u\mathrm{d}u$. Rewriting the first term on the right of this equation accordingly, it becomes

$$\frac{\mathrm{d}\rho}{\rho} = -\frac{u^2}{a_f^2} \frac{\mathrm{d}u}{u} - \frac{1}{\rho h_\rho} \sum_{i=2}^{n} h_{c_i} \mathrm{d}c_i \ ,$$

where

$$a_f^2 = \frac{-h_\rho}{h_p - 1/\rho} \ .$$

The frozen Mach number u/a_f after the normal shock is typically 0.2 or less. This means that, in the absence of dissociation, the density is practically constant along the stagnation streamline, and, with dissociation, the density change along the stagnation streamline is essentially controlled by the chemistry:

$$(\mathrm{d}\rho)_s \approx -\left(\frac{1}{h_\rho} \sum_{i=2}^{n} h_{c_i} \mathrm{d}c_i \right)_s \ .$$

This approximation makes it possible to relate the average density on the stagnation streamline to the rate at which energy is absorbed by the chemical reactions at the shock. This then appears to be the right quantity to incorporate in a new reaction rate parameter

$$\tilde{\Omega} \equiv -\frac{d}{\rho_s u_\infty} \left(\frac{1}{h_\rho} \sum_{i=2}^{n} h_{c_i} \frac{\mathrm{d}c_i}{\mathrm{d}t} \right)_s \ .$$

For a given gas mixture,

$$\tilde{\Omega} \sim \rho_s d \left(\sum_{i=2}^{n} h_{c_i} \frac{\mathrm{d}c_i}{\mathrm{d}t} \right)_s / (\rho_\infty u_\infty^3),$$

which has the physical significance of

$$\tilde{\Omega} = \frac{\text{Energy absorption rate by chemistry}}{\text{Input rate of free-stream kinetic energy}} .$$

In order to determine the value of $\tilde{\Omega}$ it is necessary to express h_ρ in terms of the conditions at the shock. This may be done by assuming that the gas mixture obeys the thermal equation of state

$$T = T(p, \rho, c_i) = \frac{p}{\rho R \Gamma} \ ,$$

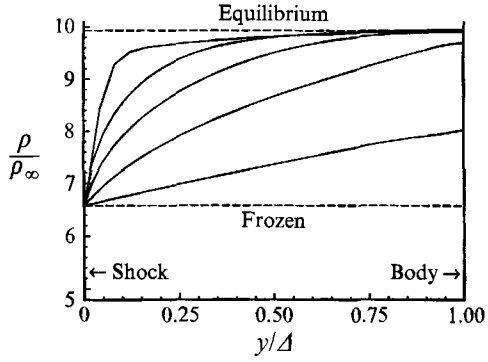

FIGURE 2. Density profile along the stagnation streamline from numerical computations for different values of the reaction rate parameter.

where

$$\Gamma = \sum_{i=1}^{n} \frac{c_i}{W_i} = \frac{1}{W} ,$$

and W_i and W are the molecular weights of species i and of the dissociated gas mixture, respectively. This leads to

$$h_\rho = -\frac{c_p p}{\rho^2 R\Gamma},$$

where

$$c_p = \sum_{i=1}^{n} c_i c_{pi} ,$$

and the c_{pi} are the specific heats at constant pressure of the constituents. The value of h_ρ at the shock can be estimated by approximating the value of p_s with $\rho_\infty u_\infty^2$, so that

$$(h_\rho)_s = -\frac{c_{ps}\rho_\infty u_\infty^2}{\rho_s^2 R\Gamma}.$$

2.2. *Density profile*

Figure 2 shows seven density profiles along the stagnation streamline obtained using an inviscid version of Candler's code plotted against y/Δ, where y is the distance from the shock. The free-stream conditions for these different profiles were the same, and the changes are brought about by successively increasing the sphere diameter. As may be seen, the profile changes in a monotonic fashion from the frozen-flow profile, with virtually constant density, to the equilibrium profile, in which all the dissociation, and therefore all the density change, occurs in the shock, and the density is again virtually constant thereafter.

Recall that the quantity that determines the stand-off distance is the average density. In fact, numerous correlations of stand-off distance with average density have been made for non-reacting flow. Upon interpretation into our variables, these give the following result:

$$\frac{\Delta}{d}\frac{\bar{\rho}}{\rho_\infty} = \tilde{\Delta}\frac{\bar{\rho}}{\rho_s} = L ,$$

where $L = 0.41$ for spheres.

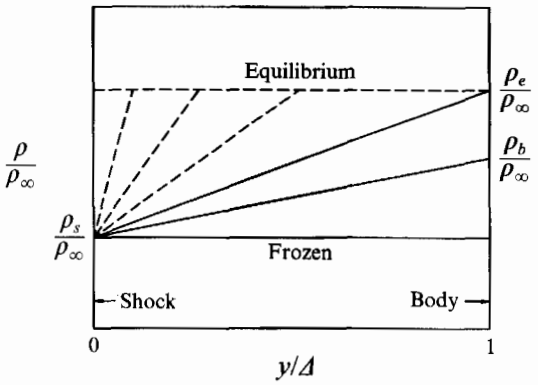

FIGURE 3. Simplified density profiles for the purpose of determining an approximate average value of the density along the stagnation streamline. ρ_b and ρ_e denote the stagnation-point density and the equilibrium density, respectively. By comparing with Fig. 2, it is clear that using this linear approximation will overestimate the average density slightly, because the actual profiles are always convex up.

Because the stand-off distance is related to the average density, the exact details of the density profile are not important and we can proceed in an approximate Kármán–Pohlhausen-type analysis by assuming linear density profiles between the shock and the body, provided that the density on the body ρ_b is smaller than the equilibrium density ρ_e. If the linear profile reaches ρ_e before the stagnation point, the density is taken to be constant thereafter at ρ_e. This clearly requires the equilibrium density to be determined and is evidently the place where the dependence of $\tilde{\Delta}$ on K (and therefore the recombination reaction) enters.

To proceed with the analysis, distinguish the cases where $\rho_b < \rho_e$ from those in which the body density is ρ_e. The slope of the density profile at the shock is determined from the dissociation rate just downstream of the shock. Figure 3 shows the simplified linear profiles.

3. Analytic solution for the stand-off distance

3.1. *The case when* $\rho_b < \rho_e$

When $\rho_b < \rho_e$, the linear profiles give

$$\left(\frac{\mathrm{d}\rho}{\mathrm{d}y}\right)_s = \frac{\rho_b - \rho_s}{\Delta} \quad \text{and} \quad \bar{\rho} = \tfrac{1}{2}(\rho_b + \rho_s) \ ;$$

$(\mathrm{d}\rho/\mathrm{d}t)_s$ can then be approximated as

$$\left(\frac{\mathrm{d}\rho}{\mathrm{d}t}\right)_s = u_s\left(\frac{\mathrm{d}\rho}{\mathrm{d}y}\right)_s = (\rho_b - \rho_s)\left(\frac{\rho_\infty}{\rho_s}\frac{d}{\Delta}\right)\left(\frac{u_\infty}{d}\right) .$$

Using the definition of $\tilde{\Omega}$ to replace $(\mathrm{d}\rho/\mathrm{d}t)_s$ leads to the quadratic equation for $\tilde{\Delta}$

$$\tilde{\Delta}^2 - (L - \tilde{\Delta})\frac{2}{\tilde{\Omega}} = 0 .$$

Only one of the two roots of this equation is physically meaningful. It is

$$\tilde{\Delta} = \frac{1}{\tilde{\Omega}}\left[-1 + \left(1 + 2L\tilde{\Omega}\right)^{1/2}\right] . \tag{3.1}$$

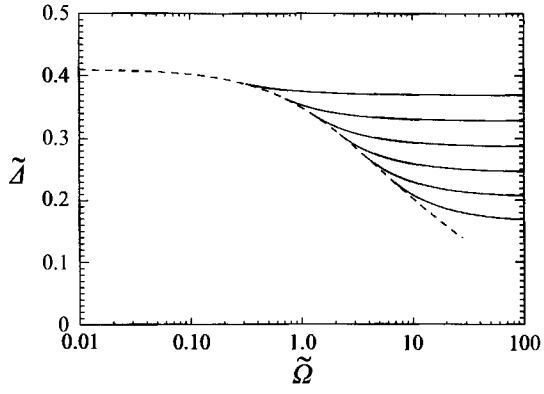

FIGURE 4. Plot of equations (3.1) (dashed line), and (3.2) (full lines) for $\rho_s/\rho_e = 0.4, 0.5, 0.6, 0.7, 0.8$ and 0.9.

This has the correct limit $\tilde{\Delta} = L$ at $\tilde{\Omega} = 0$, but will clearly fail at large $\tilde{\Omega}$, because we have to proceed differently in calculating $\bar{\rho}$ when the linear profile reaches the equilibrium density within the shock layer.

3.2. *The case when* $\rho_b = \rho_e$

For values of $\tilde{\Omega}$ that are sufficiently small, so that $\rho_b < \rho_e$, the previous section shows that $\tilde{\Delta}$ depends only on $\tilde{\Omega}$. When $\rho_b = \rho_e$, however, this is no loger true, since the equilibrium value of the density now enters the calculation of $\bar{\rho}$. Thus, a critical value of $\tilde{\Omega}$ exists for each free-stream condition, beyond which $\tilde{\Delta}$ depends on two parameters, changing in form

$$\text{from} \quad \tilde{\Delta} = f(\tilde{\Omega}) \quad \text{to} \quad \tilde{\Delta} = g(\tilde{\Omega}, \rho_e/\rho_s).$$

By proceeding as in the previous section, but this time forming the average density from the linear profile up to the point where ρ reaches ρ_e and a constant-density part with $\rho = \rho_e$ thereafter, the average density becomes

$$\frac{\bar{\rho}}{\rho_s} = \frac{\rho_e}{\rho_s} - \frac{1}{2\tilde{\Omega}\tilde{\Delta}}\left(1 - \frac{\rho_e}{\rho_s}\right)^2.$$

By using the relation between the average density and the stand-off distance, and solving for $\tilde{\Delta}$, we obtain

$$\tilde{\Delta} = \frac{\rho_s}{\rho_e}\left[L + \frac{1}{2\tilde{\Omega}}\left(\frac{\rho_e}{\rho_s} - 1\right)^2\right]. \tag{3.2}$$

Again, this may be seen to have the correct limiting value $L\rho_s/\rho_e$ when $\tilde{\Omega} = \infty$.

Equations (3.1) and (3.2) are plotted in figure 4. The curves of the two-parameter family of equation (3.2), valid for large $\tilde{\Omega}$, are nearly tangent to the single curve of equation (3.1), valid for small $\tilde{\Omega}$ at the transition point, which is different for different ρ_s/ρ_e.

The coordinates of the transition point $(\tilde{\Omega}_0, \tilde{\Delta}_0)$, can be determined explicitly as

$$\tilde{\Omega}_0 = \frac{(\rho_e/\rho_s)^2 - 1}{2L},$$

and

$$\tilde{\Delta}_0 = \frac{2L}{\rho_e/\rho_s + 1}.$$

The slopes of the two curves are not quite the same at this point. This may be seen from the fact that the average density increases less rapidly with $\tilde{\Omega}$ when the equilibrium density is reached before the stagnation point than if $\rho_e > \rho_b$ (see figure 3).

3.3. *Discussion*

The approximate theory leading to equations (3.1) and (3.2) takes account of the free-stream kinetic energy K through the appearance of the equilibrium density ρ_e. This is therefore the place where the effect of the recombination reactions enters the picture. For higher values of K, i.e. higher values of the total enthalpy h_0, the amount of energy absorbed by dissociation to equilibrium is increased, so that ρ_e/ρ_s is increased, and $\tilde{\Delta}$ is decreased. The approximate theory takes all of these effects into account in the simplest approximation. The two-part approximation of the density profile (linear plus constant) makes it necessary to distinguish between the regimes of low and high $\tilde{\Omega}$ with the two equations (3.1) and (3.2).

The two-part approximation also overestimates the average density and therefore underestimates the stand-off distance, as will be seen later. This error may be reduced significantly if the approximation for the density profile is improved, for example, by writing it as

$$\frac{\rho - \rho_s}{\rho_e - \rho_s} = 1 - \exp\left[-\frac{2\tilde{\Omega}\rho_s}{\rho_e - \rho_s}\frac{y}{\tilde{\Delta}}\right].$$

Integrating this to determine the average leads to

$$\frac{\bar{\rho} - \rho_s}{\rho_e - \rho_s} = 1 + \frac{1}{2\tilde{\Omega}\tilde{\Delta}}\left(\frac{\rho_e}{\rho_s} - 1\right)\left(\exp\left[-\frac{2\tilde{\Omega}\tilde{\Delta}\rho_s}{\rho_e - \rho_s}\right] - 1\right).$$

This is now a single equation for the average density, from which a single equation for $\tilde{\Delta}$ can be obtained by substituting in

$$\tilde{\Delta} = L\frac{\rho_s}{\bar{\rho}},$$

and solving the resulting equation for $\tilde{\Delta}$. In this case, an explicit solution is not possible, except in the two limiting cases, where the results are, of course, the same as equations (3.1) and (3.2). This refined theory is more accurate in the mid-range of $\tilde{\Omega}$. However, the simple forms of equations (3.1) and (3.2) are surprisingly accurate and the theory is much more transparent in this simpler form.

The manner in which the stand-off distance may be described in terms of the two parameters K and $\tilde{\Omega}$ is, of course, also of wider significance. It may be expected, for example, that, for a given gas, the density field in the shock layer of a blunt body will be the same for all flows in which these two parameters take the same value. The stand-off distance just serves as a convenient variable to test this concept. The success of the simple correlation stems from the fact that the influence of the chemistry on the fluid motion acts through the removal or addition of energy to or from the chemical energy store represented by the dissociated species. Thus, the important step in the

analysis is to express $\tilde{\Omega}$ in terms of the dimensionless chemical energy absorption rate.

4. Computational method

The code developed by Candler (1988) was used to compute the inviscid reacting flow over a sphere. The flow field is described by coupled partial differential equations for the conservation of species, mass, mass-averaged momentum, vibrational energy of each diatomic species and total energy. A finite-volume method using modified Steger–Warming flux-vector splitting is used to obtain the steady-state solution to these fully coupled equations for different gases. Park's semi-empirical two-temperature model and chemical kinetics model (Park 1988, 1989) was used to calculate the reaction rates for different reactions of air and nitrogen. For carbon dioxide, the chemical kinetics model of Park *et al.* (1991) was used. The scheme is implicit, using Gauss–Seidel line relaxation and is second-order accurate in the tangential direction. A compromise between efficiency in computational time and accuracy led to the use of a (56×100) grid throughout the present work. Extensive documentation of successful examples exists in reproducing experimental results in great detail, see e.g. Candler (1988), Rock, Candler & Hornung (1992), Wen & Hornung (1993), and Hornung *et al.* (1994). Since the shock values of temperature, vibrational temperatures, and density are not accessible during the experiment, the computational method provides a good way to obtain partial information about them.

The stand-off distance and the shock values of the reaction rate and density for the numerical calculation are determined from the point where the vibrational temperature reaches a maximum.

5. Experiment

5.1. *Facility*

The facility used for all the experiments described here was the free-piston shock tunnel T5 at GALCIT. The facility uses the principle of free-piston adiabatic compression of the driver gas of a shock tunnel to achieve the high shock speeds and densities required to generate high enthalpy and reaction scaling. It is capable of producing flows of air or nitrogen up to specific reservoir enthalpy h_0 of 25 MJ kg^{-1} at reservoir pressure p_0 up to 100 MPa. The shock tunnel has two additional important features. One is that the test duration is sufficiently short to avoid destruction of the machine by melting, yet long enough to provide good measurements during the steady-flow period. The other is that the gas is partially dissociated at the nozzle exit, especially in the cases of air and carbon dioxide at high specific reservoir enthalpies, where these gases also contain, respectively, some nitric oxide and carbon monoxide. A more detailed description of T5 and its performance envelope, flow quality and repeatability may be found in Hornung (1992).

5.2. *Free-stream conditions*

For the experiments, the flow was generated through a contoured nozzle of 300 mm exit diameter and 30 mm throat diameter. Using an equilibrium calculation, the specific reservoir enthalpy can be determined from the measured shock speed and the measured reservoir pressure. The nozzle flow is then computed by using an axisymmetric inviscid non-equilibrium flow code developed by Rein (1989). The calibration

	p_0 (MPa)	h_0 (MJ kg^{-1})	u_∞ (km s^{-1})	T_∞ (K)	ρ_∞ (kg m^{-3})
Nitrogen					
from	30	10.58	4.2	1390	0.0175
to	90	21.06	5.5	2760	0.0561
Air					
from	30	9.81	3.9	1340	0.0152
to	90	22.15	5.6	2930	0.0627
Carbon dioxide					
from	30	4.5	2.5	1130	0.0326
to	90	11.95	3.6	2400	0.162

TABLE 1. Range of reservoir and free-stream conditions

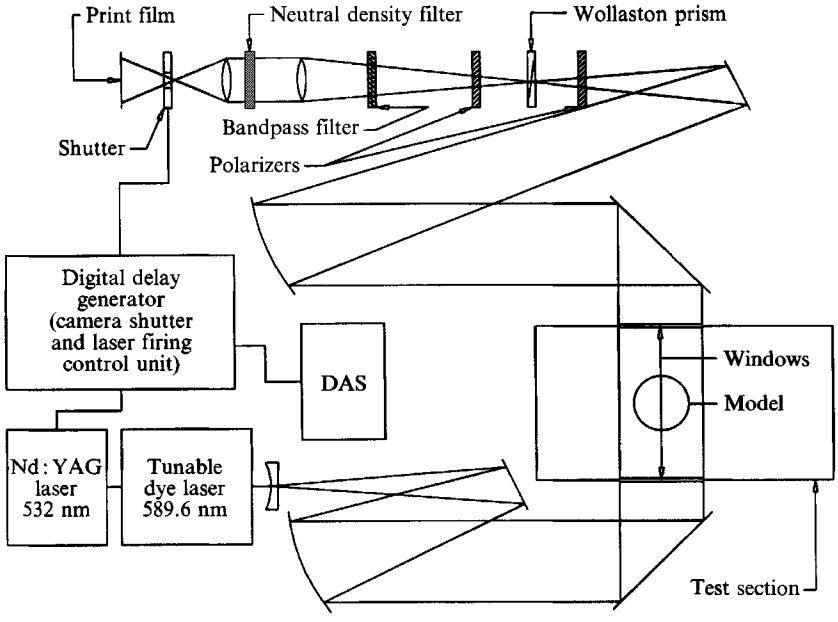

FIGURE 5. Schematic diagram of the optical arrangement. Bandpass and spatial filters are used to reduce the luminosity emitted from the test gas. The bandwidth of the bandpass filter is 10 nm centred at 590 nm for the dye laser and 10 nm centred at 532 nm for the neodymium-YAG laser.

of the free-stream conditions obtained by this method has been accomplished by measuring test section Pitot pressure distribution, see Rousset (1994) and stagnation-point heat flux, see Wen (1994).

Table 1 gives the ranges of values of the reservoir and test section conditions chosen for the present investigation. The Mach number of the free stream is about 5.5 for nitrogen, 5.3 for air and 4.6 for carbon dioxide.

5.3. *Models and flow visualization*

The models were spheres with diameters 1, 2, 3, 4 and 6 in. in order to vary the reaction rate parameter at a given tunnel condition. This has an upper limit of 6 in.

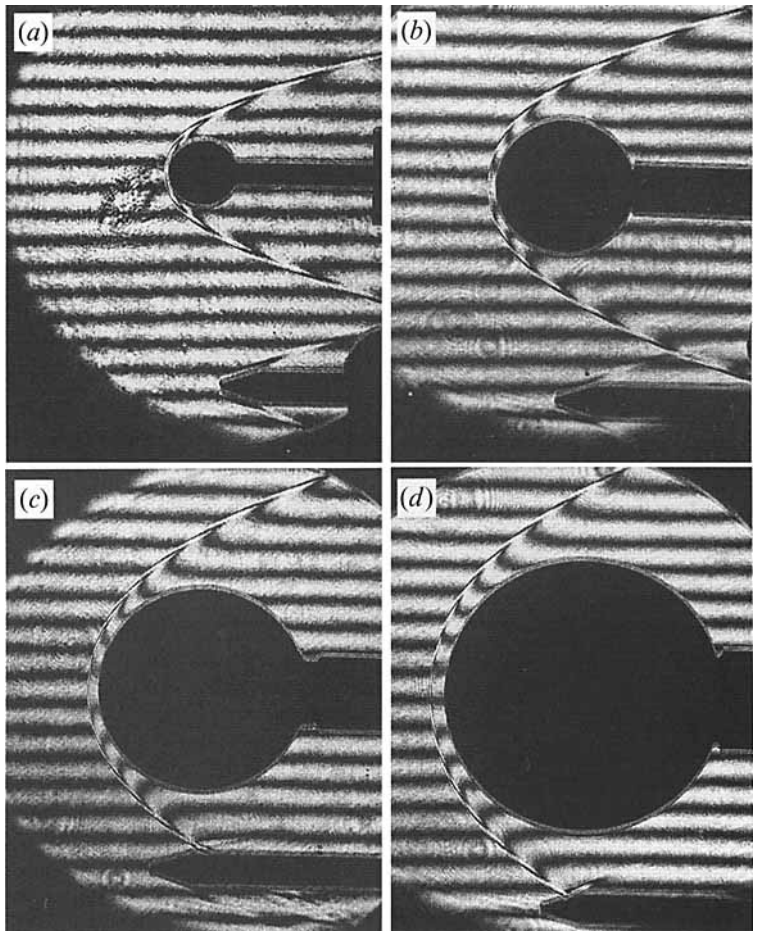

FIGURE 6. Finite fringe differential interferograms of air flow over 1, 2, 3 and 4 in. diameter spheres. $\lambda = 589$ nm. (*a*) $p_0 = 58$ MPa, $h_0 = 10.7$ MJ kg^{-1}. (*b*) $p_0 = 25$ MPa, $h_0 = 9.8$ MJ kg^{-1}. (*c*) $p_0 = 28$ MPa, $h_0 = 10$ MJ kg^{-1}. (*d*) $p_0 = 27.5$ MPa, $h_0 = 16$ MJ kg^{-1}. The blemish ahead of the bow shock wave in interferograms (a) and (b) is due to a flaw in the optical window.

because of the useful diameter of the flow, and a lower limit of 1 in. because of the resolution of the optical system. The spheres were instrumented with thermocouples to measure the surface temperature history and thus the surface heat flux, in particular at the stagnation point.

The optical system used for flow visualization is a differential interferometer shown schematically in figure 5. This instrument uses a Wollaston prism in a conventional schlieren setup and was used in the finite-fringe mode with a dye laser producing 5 mJ pulses of 6 ns duration.

6. Results

6.1. *Density field*

As an example of the interferometric results obtained, figure 6 shows a set of four finite-fringe differential interferograms of air flow over four different-size spheres, and figure 7 shows five cases of carbon dioxide flow. A large number of such measurements

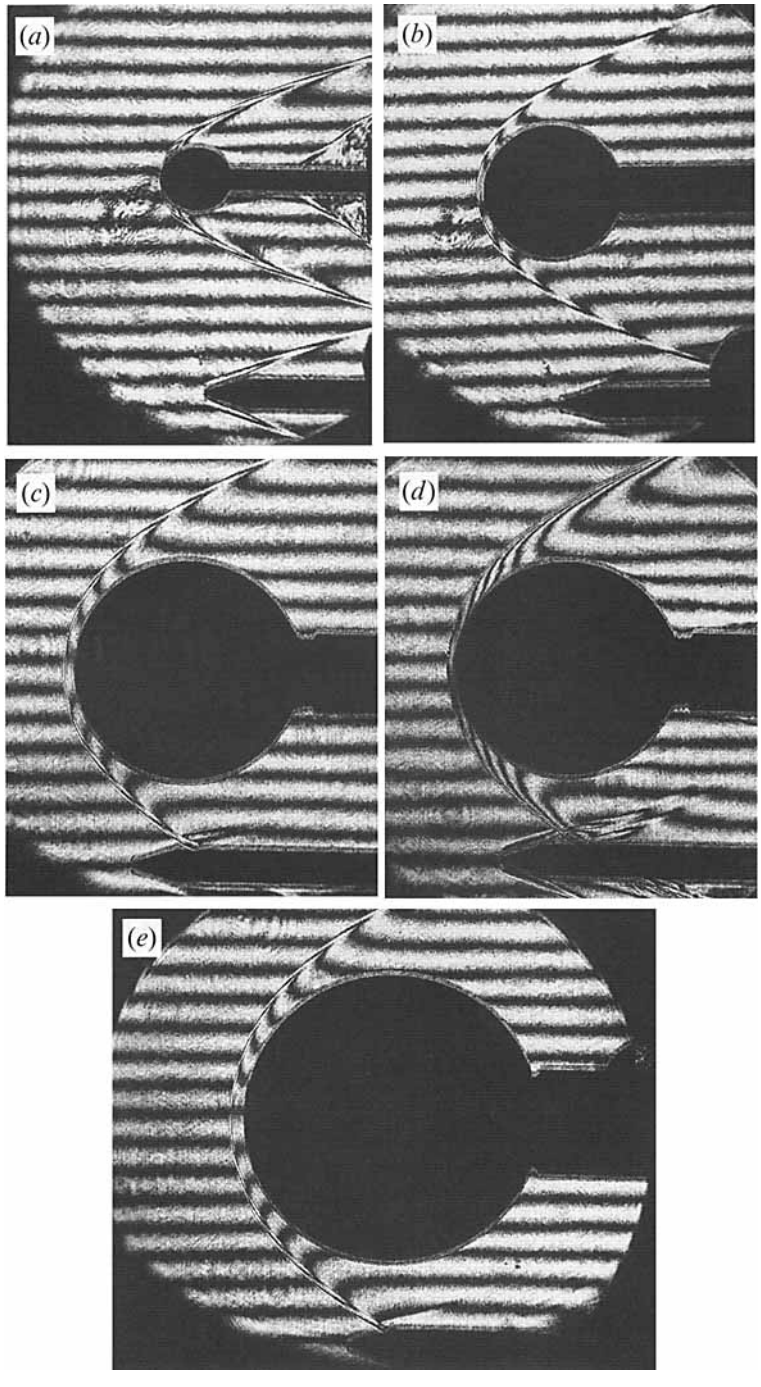

FIGURE 7. Finite fringe differential interferograms of CO_2 flow over 1, 2, 3, 3, and 4 in. diameter spheres. $\lambda = 589$ nm. (*a*) $p_0 = 55$ MPa, $h_0 = 6$ MJ kg^{-1}. (*b*) $p_0 = 25$ MPa, $h_0 = 12$ MJ kg^{-1}. (*c*) $p_0 = 25$ MPa, $h_0 = 9$ MJ kg^{-1}. (*d*) $p_0 = 55$ MPa, $h_0 = 4.6$ MJ kg^{-1}. (*e*) $p_0 = 22.5$ MPa, $h_0 = 11.4$ MJ kg^{-1}.

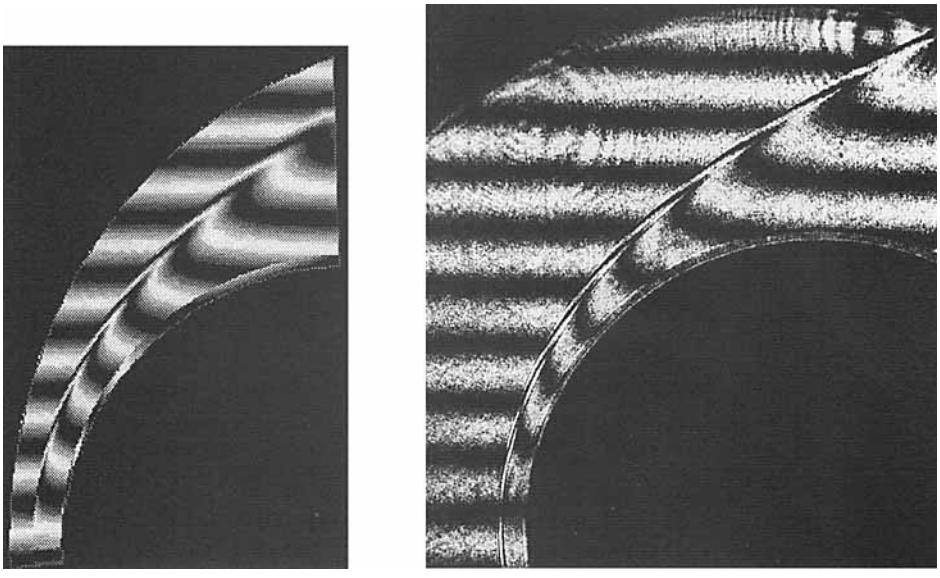

FIGURE 8. Comparison of measured (right) and computed differential interferograms in the case of air flow over a 4 in. sphere, at $p_0 = 27.5$ MPa, $h_0 = 16$ MJ kg^{-1}.

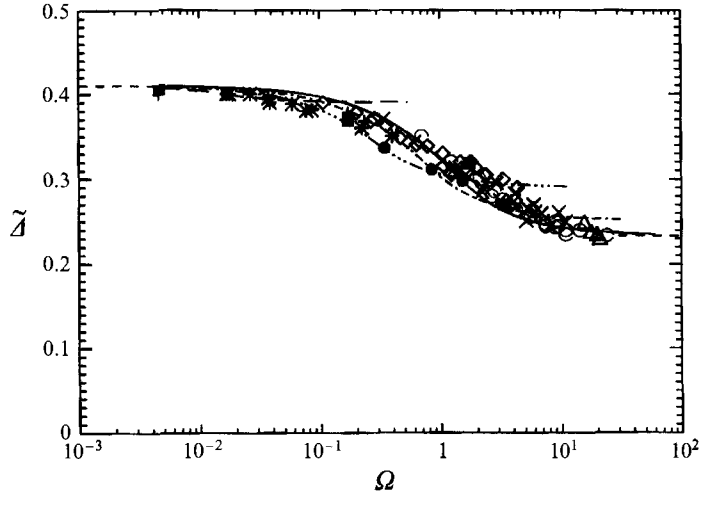

FIGURE 9. Numerical (open symbols) and experimental (full squares) results for nitrogen flow plotted in the old variables, with equations (3.1) and (3.2) superimposed. As may be seen, in these variables, the curves for different ρ_s/ρ_e are shifted relative to each other.

were taken, and compared with numerically computed interferograms. An example of such a comparison is presented in figure 8. Extensive comparisons of this kind have been made. More detail about the results of such comparisons are reported elsewhere, see e.g. Wen (1994) and Hornung, Wen & Candler (1994), Hornung (1994).

6.2. *Stand-off distance*

If equations (3.1) and (3.2) are plotted in the form $\tilde{\Delta}$ *vs.* the old reaction rate parameter Ω, in the only case where Ω can meaningfully be defined, i.e. for nitrogen,

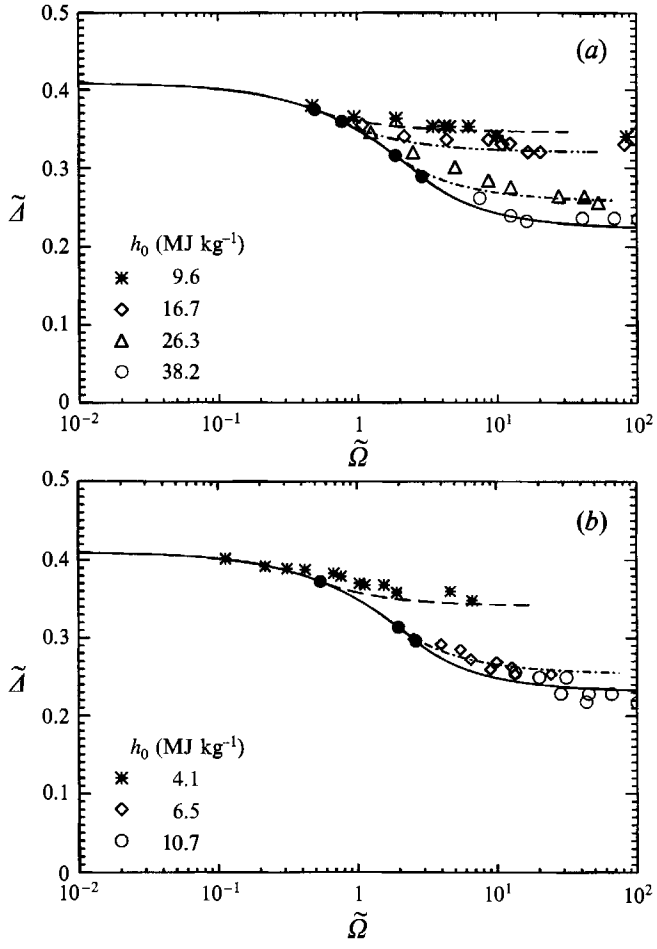

FIGURE 10. Plot of equations (3.1) and (3.2) for selected values of h_0, resulting in different values of ρ_s/ρ_e. The symbols represent computational results for (*a*) air (*b*) carbon dioxide. The full circles are the junction points of equation (3.1) and equation (3.2). Note that the theory underestimates the stand-off distance slightly, consistently with the overestimate of the average density.

the situation presented in figure 9 results. The manner in which this causes the curves for different values of ρ_s/ρ_e to be shifted relative to each other is the reason why the mistake of thinking that only one correlating parameter, Ω, is required, is easily made. The difference becomes clear when the results are plotted against $\tilde{\Omega}$, as in figure 10(*a*) which presents computational results for the case of air. Note that the value of ρ_s/ρ_e depends on h_0. Similar results are presented in figure 10(*b*) for carbon dioxide flows.

In these two plots the slight underestimate of the stand-off distance by the theory that results from the overestimate of the average density is evident in the mid-range of $\tilde{\Omega}$.

Next, we compare the experimentally measured stand-off distance in both these gases with the approximate theory, see figures 11(*a*) and 11(*b*). In the case of air, the effect appears to be much smaller than is the case in figure 10(*a*). This is because the highest value of the enthalpy in the computed cases is 38.2 MJ kg^{-1}, whereas the experiments only range up to 20.6 MJ kg^{-1}. Clearly, the nitrogen in the air is not

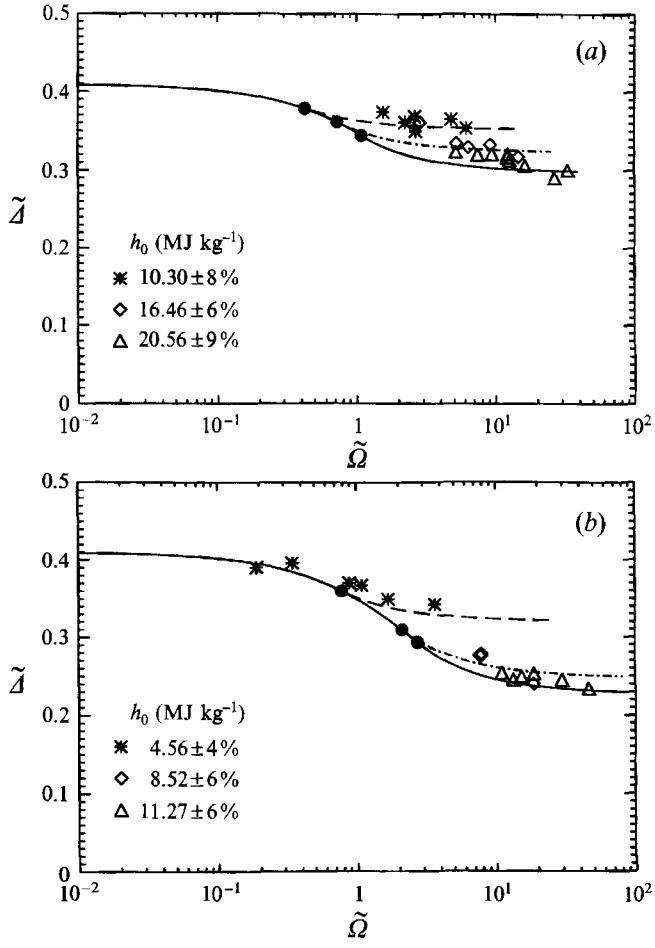

FIGURE 11. Comparison of measured dimensionless stand-off distance with the analytical theory in the case of (*a*) air flows (*b*) carbon dioxide flows.

fully dissociated at the latter value. In the case of carbon dioxide, the effect is more dramatic, because it has lower dissociation energies. In the case of air, it may also be seen that most of our experiments were conducted at conditions that are fairly close to equilibrium, since the points all lie on the large-$\tilde{\Omega}$ branch of the theory.

6.3. *Stagnation-point heat flux*

It remains to present an example of the measured stagnation-point heat flux. The high enthalpies of the flows studied can produce quite substantial values of this quantity. For example, on the small sphere, values up to 30 MW m^{-2} were obtained. The importance of measuring this quantity lies partly in the need to substantiate the reservoir specific enthalpy, h_0, which is determined indirectly from the measured shock speed in the shock tube. Figure 12 shows measurements of the stagnation-point heat flux in dimensionless form (Stanton number) plotted against the free-stream Reynolds number based on the sphere diameter for three different gases. These are compared with appropriate predictions from the correlation according to Fay & Riddell (1958). The flow and surface conditions are such that full recombination of the dissociated species may be expected to occur. (Catalytic surface.) While the experiments show

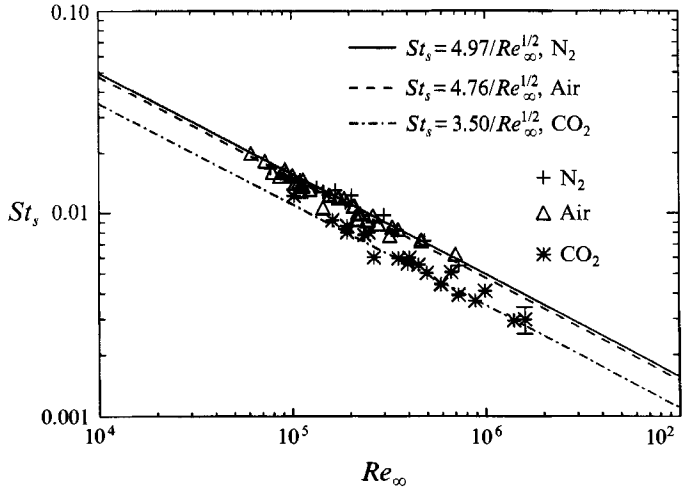

FIGURE 12. Comparison of measured dimensionless stagnation-point heat flux (symbols) with Fay & Riddell's correlation.

substantial scatter, the differences between the different gases are significant and follow the predicted differences. This provides some confirmation of the indirectly determined value of h_0.

7. Conclusions

Theoretical, numerical and experimental results on the hypervelocity dissociating flow of nitrogen, air and carbon dioxide over spheres have been presented. An approximate theory relating the dimensionless shock stand-off distance to the dimensionless total enthalpy and a reaction rate parameter corrects and extends previous relations of this kind. A previous correlation did not take into account the effects of recombination reactions which appear through the total enthalpy parameter, nor could it deal with mixtures comprising many species with many reactions. By introducing a reaction rate parameter that is a measure of the rate of energy absorption by chemical reactions immediately behind the normal shock, scaled by the rate of input of kinetic energy, it is possible to deal with complex mixtures.

Experimental results from the hypervelocity shock tunnel T5 and numerical computations support the approximate theory and give detailed information about the flow field in the form of measured and computed differential interferograms as well as stagnation-point heat transfer data.

The work leading to the material presented in this paper was sponsored by AFOSR URI grant F49620-93-1-0338 (Dr J. Tishkoff).

REFERENCES

CANDLER, G. V. 1988 The computation of weakly ionized hypersonic flows in thermo-chemical non-equilibrium. PhD thesis, Stanford University.

CANDLER, G. V. & MACCORMACK, R. W. 1988 The computation of hypersonic ionized flows in chemical and thermal non-equilibrium. *AIAA Paper* 87-1546.

FAY, J. A. & RIDDELL, F. R. 1958 Theory of stagnation point heat transfer in dissociated air. *J. Aero. Sci.* **25**, 73–85.

HORNUNG, H. G. 1972 Non-equilibrium dissociating nitrogen flows over spheres and circular cylinders. *J. Fluid Mech.* **53**, 149–176.

HORNUNG, H. G. 1992 Performance data of the new free-piston shock tunnel at GALCIT. *AIAA Paper* 92-3943.

HORNUNG, H. G., CUMMINGS, E. B., GERMAIN, P., SANDERSON, S. R., STURTEVANT, B. & WEN, C.-Y. 1994 Recent results from hypervelocity research in T5. *AIAA Paper* 94-2523.

HORNUNG, H. G., WEN, C. & CANDLER, G. V. 1994 Hypervelocity flow over spheres. *Acta Mechanica* [Suppl] **4**, 163–170.

PARK, C. 1988 Assessment of a two-temperature kinetic model for dissociating and weakly ionizing nitrogen. *J. Thermophys. Heat Transfer* **2**, 8–16.

PARK, C. 1989 Assessment of a two-temperature kinetic model for ionizing air. *J. Thermophys. Heat Transfer* **3**, 233–244.

PARK, C., JAFFE, J., HOWE, J. & CANDLER, G. V. 1991 Chemical kinetic problems of future NASA missions. *AIAA Paper* 91-0464.

REIN, M. 1989 SURF: A program for calculating inviscid supersonic reacting flows in nozzles. *GALCIT Rep.* FM 89-1 (see also *Phys. Fluids* A **4**, 873–886, 1992).

ROCK, S. G., CANDLER, G. V. & HORNUNG, H. G. 1992 Analysis of thermo-chemical non-equilibrium models for carbon dioxide flows. *AIAA Paper* 92-2852.

ROUSSET, B. 1995 Calibration and study of the contoured nozzle of the T5 free-piston hypervelocity shock tunnel. AeE thesis, Graduate Aeronautical Laboratories, Caltech.

WEN C.-Y. 1994 Hypervelocity flow over spheres. PhD thesis, Graduate Aeronautical Laboratories, Caltech.

WEN, C. & HORNUNG, H. G. 1993 Experiments on hypervelocity dissociating flow over spheres. *Proc. 19th Intl Symp. on Shock Waves, Marseille*, to appear.